

Migration and accumulation of bacteria with chemotaxis and chemokinesis

Theresa Jakuszeit,^{1,*} James Lindsey-Jones,¹ François J. Peaudecerf,² and Ottavio A. Croze^{1,†}

¹*Cavendish Laboratory, University of Cambridge, Cambridge CB3 0HE, U.K.*

²*Institute of Environmental Engineering, Department of Civil, Environmental and Geomatic Engineering, ETH Zürich, 8093 Zürich, Switzerland*

(Dated: August 15, 2019)

Bacteria can chemotactically migrate up attractant gradients by controlling run-and-tumble motility patterns. In addition to this well-known chemotactic behaviour, several soil and marine bacterial species perform chemokinesis: they adjust their swimming speed according to the local concentration of chemoattractant, with higher speed at higher concentration. A field of attractant then induces a spatially varying swimming speed, which results in a drift towards lower attractant concentrations – contrary to the drift created by chemotaxis. Here, to explore the biological benefits of chemokinesis and investigate its impact on the chemotactic response, we extend a Keller-Segel-type model to include chemokinesis. We apply the model to predict the dynamics of bacterial populations capable of chemokinesis and chemotaxis in chemoattractant fields inspired by microfluidic and agar plate migration assays. We find that chemokinesis combined with chemotaxis not only enhances the population response with respect to pure chemotaxis, but also modifies it qualitatively. We conclude presenting predictions for bacteria around dynamic finite-size nutrient sources, simulating, e.g., a marine particle or a root. We show that chemokinesis can reduce the measuring bias that is created by a decaying attractant gradient.

INTRODUCTION

Many bacteria are able to swim by rotating helical flagella distributed on their cell body, and control their swimming pattern by modulating the speed or direction of rotation of their flagellar motors. For example, in the model run-and-tumble motion of *Escherichia coli* [1], a bacterium swims approximately straight in a ‘run’ by rotating its flagella in a bundle. When some flagella change their rotation direction, the bundle comes apart and the cell randomly changes direction in a ‘tumble’. In the absence of external bias, this microscopic pattern resembles a random walk, and leads to macroscopic diffusion of a bacterial population. In the presence of a chemical gradient, the random walk is biased, a response known as chemotaxis. As illustrated in Fig. 1(a), a bacterium achieves the biased motion up a gradient of attractant by varying the frequency of tumbles in its random walk: if the bacterium moves up the gradient, the tumbling rate α decreases and, thus, the run length increases, while the swimming speed remains constant.

The run-and-tumble model was originally introduced for enteric bacteria such as *E. coli* and *Salmonella typhimurium* [2, 3], which commonly live in nutrient-rich environments, such as the gut. Marine and soil bacteria, however, often experience heterogeneous and nutrient-scarce environments, and have been found to display different motility patterns. For example, several species living in these harsher environments respond to higher concentrations of attractant by increasing their speed [4–6]. This response, known as ‘chemokinesis’, modifies the swimming speed in response to the local chemical concentration without affecting the tumbling rate, as illustrated in Fig 1(b). A positive chemokinetic response leads to a

higher swimming speed at higher attractant concentrations, whereas a negative response lowers the speed at those concentrations.

The biological significance of the chemokinetic response of some marine and soil bacteria has yet to be fully elucidated. Based on the environment that chemokinetic bacteria have been found in, (positive) chemokinesis might be beneficial in heterogeneous environments with scarce sources of nutrients (attractants). For example, alga-sized microbeads coated with various amino acids were used to study the response of marine bacteria to point-like sources of attractants [4]. All marine bacteria studied were observed to accumulate in bands around the point-like sources while displaying a chemokinetic response. Furthermore, chemokinesis could allow marine bacteria to track algae, helping to foster symbioses with these microorganisms, as well as permitting to respond quickly to short bursts of nutrients, such as those generated from lysing algae [7]. Another example of a chemokinetic marine bacterium is the coral pathogen *Vibrio coralliilyticus*. Microfluidic experiments on this pathogenic bacterium in combination with mathematical modelling have suggested that the maximum accumulation in response to chemical cues produced by heat-stressed coral hosts is larger and is reached faster than in the absence of chemokinesis [5, 8]. As heat-stressed corals are more susceptible to pathogens, chemokinesis could be a crucial evolutionary advantage in oceans heating up due to climate change.

Recent interest in chemokinesis has also been sparked by synthetic microswimmers, such as Janus particles. Janus particles are synthetic colloids in a bath of fuel (e.g. H_2O_2) that propel due to an asymmetric chemical reaction on their surface [9]. These particles show a positive chemokinetic response since their swimming

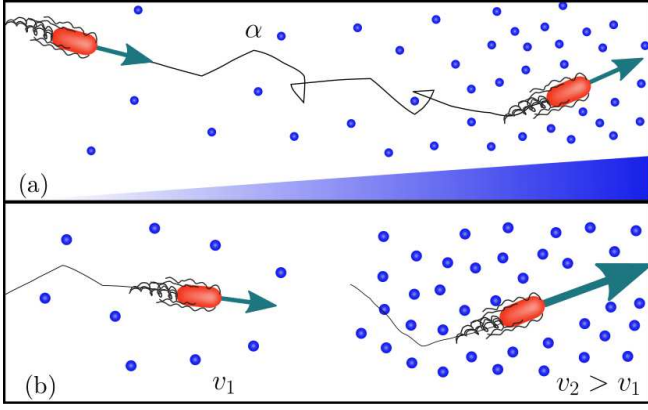


FIG. 1: Chemotaxis vs. chemokinesis: (a) Chemotaxis is the biased movement of bacteria up a chemical gradient of attractant by reducing the tumbling rate α and, thereby, increasing the length of runs in a favourable direction. (b) Positive chemokinesis leads to an increase in swimming speed v in response to an increase in the local attractant concentration.

speed increases with increasing fuel concentration [10], and therefore accumulate in areas of lower fuel concentration.

To date, theoretical work on the combination of positive chemokinesis and chemotaxis has focussed on single-cell level using agent-based models [5, 11, 12]. The chemokinetic response of the marine pathogen *Vibrio cholera* has been modelled as a step increase in swimming speed beyond a threshold attractant concentration [11]. This model was used to analyse the chemotactic response to a transient attractant gradient in a microfluidic device after an initial release of attractant. The chemotactic index (i.e. the enhancement in cell concentration over a control region) suggests that chemokinesis enables a stronger and faster response. However, the spatio-temporal response at the population level has not been analysed in detail.

In this work, we use a continuum model to study the spatio-temporal dynamics of bacterial populations with chemokinetic and chemotactic responses. We incorporate chemokinesis into the standard Keller-Segel model for chemotaxis by deriving the model from microscopic run and tumble dynamics. The model is then used to obtain analytical conditions for chemokinetic drift, and solved numerically for three different example attractant distributions that are inspired by existing experimental systems.

MODEL

We derive a model for chemotaxis in combination with positive chemokinesis by considering a one-dimensional

system in which a cell can move either to the right or left with speed v . In this system, a right (left) moving particle changes direction with rate α_R (α_L). Following [13], the one-particle probability density for bacteria evolves according to $\partial b / \partial t = -\partial J / \partial x$, and the bacterial flux J can be derived as

$$J(x) = -D_b(x) \frac{\partial b}{\partial x} + V(x)b \quad (1)$$

$$\text{with } D_b(x) = \frac{v^2}{2\alpha}, \quad V(x) = -\frac{v}{\alpha} \frac{\partial v}{\partial x} + \frac{v}{2\alpha}(\alpha_L - \alpha_R), \quad (2)$$

where $\alpha_R + \alpha_L = 2\alpha$. This is a drift-diffusion equation with bacterial diffusion coefficient $D_b(x)$ and drift velocity $V(x)$. In the case of a spatially varying swimming speed $v(x)$ and a constant tumble rate α , the bacterial diffusivity is spatially varying (see Eq. (2)) and we can rewrite the bacterial flux as

$$J(x) = -D_b(x) \frac{\partial b}{\partial x} - \frac{b}{2} \frac{\partial D_b(x)}{\partial x} + \frac{v}{2\alpha}(\alpha_L - \alpha_R)b. \quad (3)$$

We will now connect the bacterial flux to the commonly used Keller-Segel model of chemotaxis.

Chemotaxis

For chemotactic populations, the drift-diffusion equation of the one-particle probability density is coupled to an attractant density field c via a drift velocity. The second term of the drift velocity V in Eq. (2) depends on the difference between tumble rates, which depends on chemical gradients and can, therefore, be identified as chemotactic drift velocity, V_χ . In the standard Keller-Segel model it is phenomenologically asserted that this chemotactic drift velocity is proportional to the change in the chemical attractant in space, $V_\chi = \chi \nabla f_\chi$, where χ is the chemotactic sensitivity and f_χ is a function of c that ensures that the chemotactic drift is biased towards higher attractant concentrations [14]. This definition of the chemotactic drift velocity assumes that the chemical attractant profile changes in space but not in time. However, as mentioned, known chemokinetic bacteria inhabit dynamic environments, such as in the ocean. As pointed out by Hein et al [15] the effective gradient perceived by a bacterium changes in a temporally varying attractant profile depending on the direction of its run. Consider a source of attractant at one point of space, and the associated negative gradients of concentration as one gets away from it. If these gradients are steady in time, for example as in a microfluidic setting, a bacterium exploiting the attractant landscape will correctly detect the gradient and swim towards the source, as in

standard chemotaxis. However, if the source corresponds to a single point-like release of a finite mass of attractant, and the concentration at the source position also decays due to diffusion, a bacterium travelling toward the source perceives a smaller increase (or even a decrease) in concentration compared to the steady case. On the other hand, a bacterium moving away from the source perceives a decrease, which is reduced in magnitude compared to the steady case. We show in Appendix how this influences the mean run length of a bacterium, and, in light of this, modify the chemotactic drift speed to

$$V_\chi = \chi \left(\nabla f_\chi - \frac{1}{v} \partial_t f_\chi \right). \quad (4)$$

Thus, a dynamic attractant gradient can reduce the drift up a gradient. For the response function, we may choose, for example [16],

$$f_\chi = \frac{c(x, t)}{c(x, t) + k_\chi}. \quad (5)$$

Following [17], the microscopic swimming parameters v and α can be related to the macroscopic parameter χ (see Appendix for details) as

$$\chi = \frac{v^2}{\alpha} \beta, \quad (6)$$

where β is constant dependent on the chemotactic response (again, see Appendix for details).

Chemokinesis

In this section we consider how chemokinesis can be modelled. We can modify Eq. (6) to include chemokinesis (a spatially varying swimming speed) to give

$$\chi(x) = \chi_0 \frac{v(x)^2}{v_0^2}, \quad (7)$$

in which the subscript refers to the parameters in the absence of chemokinesis (the interested reader can find a detailed derivation in Appendix). Here we assumed that the swimming speed is constant during a run.

In addition to modifying the chemotactic drift χ , the spatially varying swimming speed causes a chemokinetic drift with a speed given by

$$V_k = -\frac{v}{\alpha} \frac{\partial v}{\partial x}, \quad (8)$$

which drives the cells towards regions of lower speed [13].

Next we consider how to quantify the chemokinetic coupling between speed and local concentration of attractant. We need to make assumptions about the relationship between speed and attractant concentration, as experimental studies have not been carried out to provide this. Firstly, we assume that cells swim at a base level speed, v_0 . Secondly, we reasonably posit that chemokinesis monotonically increases the swimming speed up to a maximum speed denoted as $v_0 + v_c$. The dynamics between these limits are given by an unknown chemokinetic response function. For example, a Michaelis-Menten type equation

$$v(x) = v_0 + v_c \frac{c(x)}{c(x) + k_c} \quad (9)$$

could satisfy the above assumptions. The speed monotonically increases from v_0 to the maximum $v_0 + v_c$ ($v_c > 0$) with increasing attractant concentration, where the half-maximum speed is reached at the attractant concentration k_c . Although Eq. (9) satisfies all the assumptions we have made, this particular chemokinetic response function is limited by the absence of an inflection point. The chemokinetic drift velocity scales with the gradient of swimming speed, $\frac{\partial v}{\partial x} = \frac{\partial v}{\partial c} \frac{\partial c}{\partial x}$, which is maximised at an inflection point. Thus, we choose a Hill-type equation

$$v(x) = v_0 + v_c \frac{c(x)^n}{c(x)^n + k_c^n} \quad (10)$$

to approximate the chemokinetic response. The Hill parameter n allows us to introduce an inflection point and change the gradient $\partial v / \partial c$. As can be seen from Fig 2, the speed increases monotonically with increasing attractant concentrations c for all n and $v_c > 0$. Note that upon setting $n = 1$, one recovers Eq. (9); for $n \rightarrow \infty$, Eq. (10) approaches a step function, which has been used previously to approximate the chemokinetic response [5, 11].

Finally, as we are interested in modelling growing populations, the bacteria are also assumed to undergo logistic growth, which comprises growth and death terms [16]. The full model equations for the chemical attractant field and the bacterial population field, therefore, are

$$\frac{\partial c}{\partial t} = D_c \frac{\partial^2 c}{\partial x^2} - k_g g(c) \frac{b}{Y} \quad (11a)$$

$$\frac{\partial b}{\partial t} = \frac{\partial J}{\partial x} + k_g \left(g(c) - \frac{b}{k_b} \right) \quad (11b)$$

$$J(x) = \frac{v^2}{\alpha} \frac{\partial b}{\partial x} + \frac{v}{\alpha} \frac{\partial v}{\partial x} b - \chi(x) \left(\nabla f_\chi - \frac{1}{v} \partial_t f_\chi \right), \quad (11c)$$

where $g(c)$ is chosen as a Monod-type growth function $g(c) = c/(c + k_s)$ with the half-saturation constant k_s .

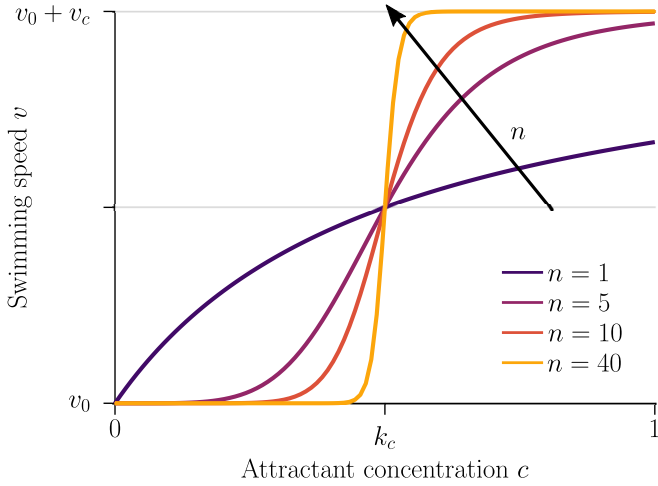


FIG. 2: Chemokinetic response function. The swimming speed increases from a reference speed, v_0 , by at most v_c , depending on the local concentration of the attractant according to a Hill type function. The parameter n determines the strength of the gradient at the half-saturation concentration, k_c .

Let us summarise the effects of chemokinesis in our model. A spatially varying speed affects all three terms of the bacterial flux J in Eq. (11c) as: (i) there are regions with a higher diffusivity since $D_b \sim v^2$ (first term); (ii) it introduces a drift where $\partial v / \partial x \neq 0$ (second term); and (iii) there are regions with a larger chemotactic drift as $\chi \sim v^2$ (third term).

Non-dimensionalisation

The system of partial differential equations (11) is non-dimensionalised using the characteristic time and length scales $t_0 = k_g^{-1}$ and $x_0 = \sqrt{t_0 D_b^0}$, where the bacterial diffusivity is $D_b^0 = v_0^2 \alpha^{-1}$. We rescale the attractant and bacterial densities by their respective initial densities, c_0 and b_0 . The system of PDEs in dimensionless form thus reads

$$\frac{\partial C}{\partial T} = N \nabla^2 C - HB \frac{C}{C + K_S} \quad (12a)$$

$$\frac{\partial B}{\partial T} = \nabla J + B \left(\frac{C}{C + K_S} - B \right) \quad (12b)$$

$$J = \mathcal{V}(X)^2 \nabla B + V_k B - V_\chi B \quad (12c)$$

$$V_k = \mathcal{V}(X) \frac{n \eta \omega^n C^{n-1}}{(C^n + \omega^n)^2} \nabla C \quad (12d)$$

$$V_\chi = \mathcal{V}(X)^2 \frac{\delta_0 K_\chi}{(C + K_\chi)^2} \left(\nabla C - \frac{\zeta}{\mathcal{V}(X)} \frac{\partial C}{\partial T} \right) \quad (12e)$$

with non-dimensional parameters $B = b/b_0$, $C = c/c_0$, $N = D_c/D_b^0$, $H = b_0/(Y c_0)$, $K_S = k_s/c_0$, $\eta = v_c/v_0$,

$\omega = k_c/c_0$, $\delta_0 = \chi_0/D_b^0$, $\zeta = v_0/(\alpha x_0)$ and $K_\chi = k_\chi/c_0$. The non-dimensional speed function in Eq. (12) is

$$\mathcal{V}(X) = 1 + \eta \frac{C^n}{C^n + \omega^n}, \quad (13)$$

where η is the maximum increase in swimming speed, ω is the attractant concentration at which the half maximum speed increase is reached, and n is the Hill parameter. Note that ω corresponds to the inflection point of Eq. (13).

Finally, the model is extended to the 2D axisymmetric case by introducing polar coordinates as

$$\nabla B = \frac{\partial B}{\partial R} \quad (14a)$$

$$\nabla^2 B = \frac{\partial^2 B}{\partial R^2} + \frac{1}{R} \frac{\partial B}{\partial R}, \quad (14b)$$

and the equivalent equations for the chemical field, C . The details of the numerical solution and simulations of the model are described in appendix , including a summary of parameters used. In section we will present the simulation results for three different types of attractant gradient.

Condition for dominant chemokinetic drift

Before solving the extended Keller-Segel model numerically, we can use Eq. (12) to analytically derive a condition on the relative importance of chemokinetic and chemotactic contributions to the drift of the bacterial population. The drift due to a spatially varying swimming speed causes cells to accumulate in regions where they have low speeds. For $\eta > 0$, by construction of the velocity function (13), the speed is low at low attractant concentrations. The chemotactic drift, on the other hand, is directed towards higher attractant concentrations by virtue of Eq. (5). Hence, the bacterial density is governed by two competing drifts, as can be seen from the opposing signs in Eq. (12c). If the chemokinetic drift is larger than the chemotactic drift for a large part of the spatial domain, this could lead to accumulation at low attractant concentrations, instead of the biologically-desirable accumulation at high concentrations. Assuming a stationary attractant profile, we have from Eq. (12d) and (12e) that the chemokinetic drift is larger than the chemotactic drift if

$$\frac{n \eta \omega^n}{(C^n + \omega^n)^2} \mathcal{V}^{-1} C^{n-1} > \frac{\delta_0 K_\chi}{(C + K_\chi)^2} \quad \forall X \in \Omega, \quad (15)$$

where Ω is the spatial domain. Furthermore, from Eq. (13) (and Fig. 2), we know that the gradient is max-

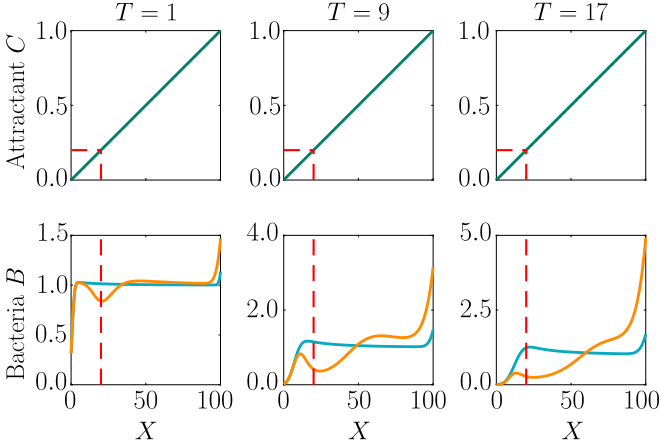


FIG. 3: Steady linear gradient. Bacterial response (bottom row) to a fixed linear attractant gradient (top row) using pure chemotaxis (blue curve) versus chemotaxis with chemokinesis (orange curve) for three time points. The position at which $C = \omega$ is highlighted by a dotted red line. Parameters $H = 0$, $N = 0$, $K_\chi = 0.53$, $\delta_0 = 50$, $\eta = 2$, $\omega = 0.2$, $n = 5$, $T = 1, 9, 17$.

imum at the half-saturation constant ω . Thus, we evaluate condition (15) with $C = \omega$, which yields the condition

$$n > \frac{4\delta_0\omega K_\chi}{(\omega + K_\chi)^2} \left(\frac{1}{\eta} + \frac{1}{2} \right) \forall X \in \Omega : C(X) = \omega. \quad (16)$$

If the Hill parameter n exceeds this threshold, the chemokinetic drift is predicted to be larger than the chemotactic drift at the attractant concentration $C^* = \omega$ for $\eta > 0$. Note that, for a step function, condition (16) is always met at the threshold concentration $C^* = \omega$ since $n \rightarrow \infty$. Conversely, if $\eta < 0$ (i.e. modelling a negative chemokinetic response), condition (16) will never be met as the chemotactic and chemokinetic drift have the same direction (chemokinesis in this case is stabilising).

RESULTS

Steady linear gradient

The full model Eq. (12) includes the effect of growth and consumption as well as chemotaxis and chemokinesis. Thus, any change in the spatial distribution of the bacterial population due to chemotaxis and chemokinesis will feed back onto the attractant distribution due to consumption by the bacteria. In order to identify the influence of chemokinesis without such additional complications, we first solve the model for a steady attractant gradient, i.e. $\partial C / \partial T = 0$. We furthermore assume a linear gradient such that $\partial C / \partial X = \text{const}$ and ignore consumption, and thus population growth. This situation might be achieved experimentally in microfluidic

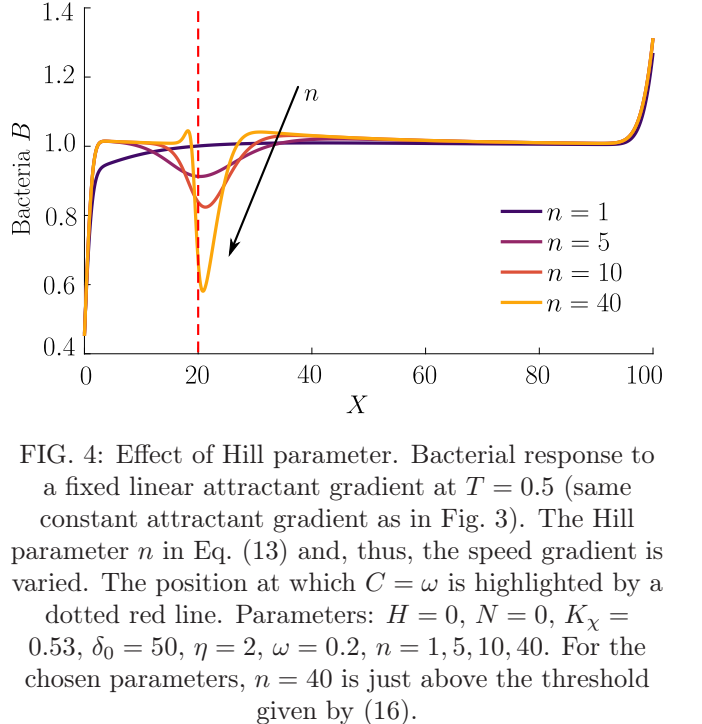


FIG. 4: Effect of Hill parameter. Bacterial response to a fixed linear attractant gradient at $T = 0.5$ (same constant attractant gradient as in Fig. 3). The Hill parameter n in Eq. (13) and, thus, the speed gradient is varied. The position at which $C = \omega$ is highlighted by a dotted red line. Parameters: $H = 0$, $N = 0$, $K_\chi = 0.53$, $\delta_0 = 50$, $\eta = 2$, $\omega = 0.2$, $n = 1, 5, 10, 40$. For the chosen parameters, $n = 40$ is just above the threshold given by (16).

devices [18], where the gradient may be fixed and bacterial growth can be neglected on experimental timescales short compared to growth timescales $\sim k_g^{-1}$.

Fig. 3 compares the response of a purely chemotactic population to the response of a chemotactic-chemokinetic population. Chemokinesis leads to a stronger and faster accumulation than in the purely chemotactic case. At the critical concentration, $C = \omega$, however, the chemokinetic drift holds back a subset of the population because it is directed towards lower attractant concentrations. This can be seen in the form of an accumulation of cells at low attractant concentrations. As the chemotactic sensitivity parameter, δ_0 , is large in this simulation, the population subset overcomes the drift and accumulates at high attractant concentrations at long times. However, if condition (16) is fulfilled, the chemokinetic drift is larger than the chemotactic drift. Thus, there is a subpopulation driven to small attractant concentrations by chemokinesis. The effect of varying the Hill parameter n in Eq. (13) is illustrated in Fig. 4. For the parameters chosen in Figure 3, condition (15) is met for $n > 39.78$.

As the attractant concentration is fixed, we can determine a steady-state for the bacterial population, i.e. by setting $\partial B / \partial T = \partial J / \partial X = 0$. Due to the homogeneous Neumann boundary conditions of the problem, we have $J = 0$ in Eq. (12), which yields the differential equation

$$\frac{\partial B}{\partial X} + B \left[\frac{1}{2D} \frac{\partial D}{\partial X} - \delta_0 \frac{d}{dX} \left(\frac{C}{C + K_\chi} \right) \right] = 0, \quad (17)$$

where we used $D(X) = \mathcal{V}(X)^2$. This equation can be

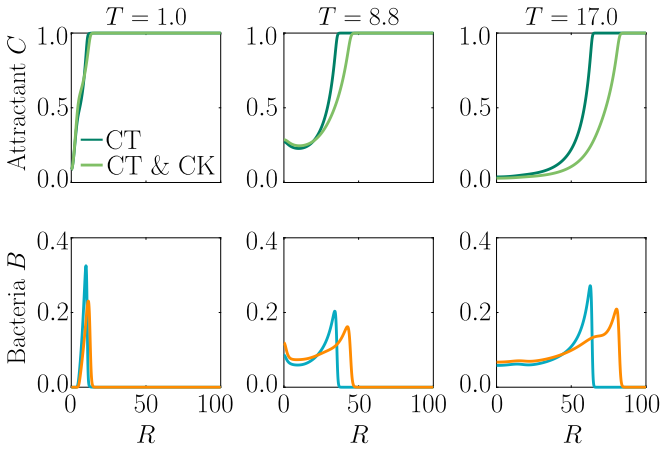


FIG. 5: Self-generated gradient. Bacterial populations (bottom row) create an attractant gradient (top row) via consumption, which they respond to with chemotaxis (blue curve) or chemotaxis-chemokinesis (orange curve). Chemokinesis leads to a faster but also broader, less pronounced bacterial wave. Parameters $H = 3.5$, $K_S = 1$, $N = 0.5$, $K_\chi = 0.53$, $\delta_0 = 105$, $\eta = 0.5$, $\omega = 0.5$, $n = 5$, $T = 1, 8.8, 17$

integrated to give the steady-state

$$\frac{B}{B^*} = \frac{\mathcal{V}^*}{\mathcal{V}} \exp \left\{ \delta_0 \left(\frac{C}{C + K_\chi} - \frac{C^*}{C^* + K_\chi} \right) \right\}, \quad (18)$$

where B^* , C^* , \mathcal{V}^* are reference values at a chosen reference point X^* . It is thus clear that, in addition to the influence on the dynamics, chemokinesis affects the steady-state solution via the term $\mathcal{V}^*/\mathcal{V}$, where \mathcal{V} varies in space due to chemokinesis. In the case of chemokinesis but no chemotaxis (i.e. $\delta_0 = 0$), the steady-state is determined by the inverse of the speed distribution, i.e. the bacteria accumulate at low speed, as expected and shown previously [13, 19]. For non-zero δ_0 , if the speed is uniform in space, $\mathcal{V}^*/\mathcal{V} = 1$ and Eq. (18) reduces to the chemotactic steady-state solution. The exponential term in Eq. (18) represents the chemotactic contribution to the steady state, which does not depend on the swimming speed. Thus, the increase in chemotactic sensitivity χ (see Eq. (7)) must be balanced by the increase in diffusivity at steady state in a fixed chemical gradient. However, chemokinesis still affects the steady state via the term $\mathcal{V}^*/\mathcal{V}$. This chemokinetic effect in the steady-state may only be detectable in experiments with small $\delta_0 = \chi_0/D_b$, since the chemotactic exponential term will dominate $\mathcal{V}^*/\mathcal{V}$ for large δ_0 .

Self-generated gradient: agar plate

We now consider an evolving attractant field with consumption and growth of bacteria. The attractant is ini-

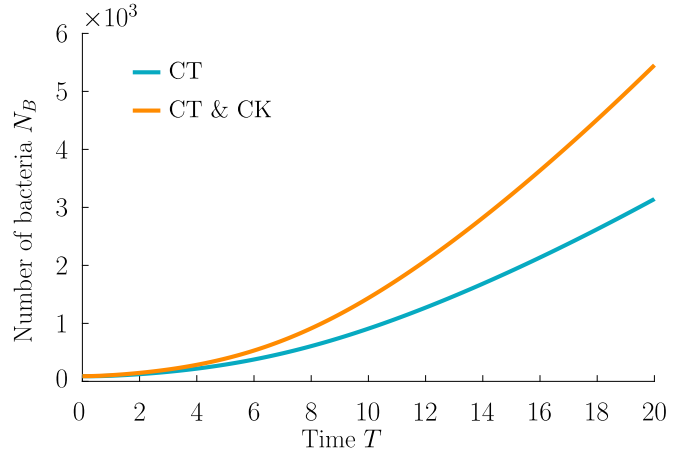


FIG. 6: Population growth. The size of the populations in Fig. S2 is the bacterial density integrated over the simulation domain. Faster travelling waves of the chemokinetic-chemotactic population (orange curve) also induce a faster population growth due to consumption of nutrients, compared to the purely chemotactic population (blue curve). Parameters as in Fig. S2

tionally uniformly distributed in a 2D axisymmetric setting. This set-up is reminiscent of the classical agar plate experiments, in which bacteria are inoculated in the centre of a nutrient agar plate, see e.g. [16, 20]. While growing and consuming nutrient, the population creates a gradient of attractant, which it then follows outwards in a chemotactic wave. The attractant profile is a travelling wave itself, and we assume here that the profile relative to the bacterial travelling wave is stationary, i.e. $\zeta = 0$ in the chemotactic drift (12e).

As can be seen from Fig. S2, a chemotactic-chemokinetic bacterial population develops a faster travelling wave compared to the purely chemotactic case. The larger expansion rate of the wave is caused by the chemokinetic increase in swimming speed for bacteria in the wave front and the increase in chemotactic sensitivity. However, the increased speed also increases the diffusivity of the bacterial population around the wave front. The peak of the chemotactic-chemokinetic wave is, therefore, smaller, and the wave more spread out, with a plateau following the travelling wave peak, as can be seen in the third lower panel of Fig. S2. This observation might explain why in agar plate experiments testing for chemotaxis, chemokinetic species such as *Sinorhizobium meliloti* lack the sharp bands [21, 22], which are known to be a hallmark of chemotaxis for other species, e.g. *E. coli* [16, 20].

Chemokinesis confers an additional evolutionary advantage in form of increased population growth as can be seen in Fig. 6, which shows the integrated number of cells over time. At any point in time, the chemotactic

population is smaller than the chemotactic-chemokinetic population.

Transient source

It has been suggested that chemokinesis is beneficial in nutrient-sparse environments such as the ocean or soils, which have a very heterogeneous distribution of nutrients [4, 7]. A localised burst of nutrient may, e.g., occur in the sea if algae/phytoplankton lyse and release their content, as has been recently studied in the laboratory [23], or when marine particles exude plumes of nutrients [24]. In soil, plant roots exude sugars and other potential nutrients, which locally create a high concentration of chemical attractants. In the following, we consider a single strong pulse of attractant originating from a finite-size axisymmetric source that dissipates via diffusion, modelling a potential dynamic environment around roots or marine particles. The attractant profile that develops is $C(R, T) = S/\sqrt{4\pi NT} \exp(-R^2/4NT)$, which is illustrated in Fig. S3 (top row). To model such a transient attractant profile, we need to include the chemotactic drift velocity, $V_\chi = \chi(\nabla f_\chi - \partial_t f_\chi/v)$, modified to account for the effective gradient perceived by bacteria as they traverse the temporally varying pulse (see Appendix).

As can be seen from Fig. S3, bacteria with chemotaxis and chemokinesis display a faster and stronger response than for those with chemotaxis alone. This strong accumulation occurs even though diffusivity close to the source is higher for these bacteria. Temporal variations in the concentration ($\sim \partial_t f_\chi$) need to be considered when modelling the chemotactic response for these transient pulses. Indeed, the tumble rate for a bacterium travelling up/down the gradient is $\tau^{L,R} \propto \pm(v\nabla f_\chi - \partial_t f_\chi)$ (see Appendix). Thus, for chemokinetic bacteria with higher v , the temporal perturbation to the chemotactic bias of tumbles is reduced, increasing the accuracy of the chemotactic response. This effect contributes to the stronger accumulation of chemotactic-chemokinetic bacteria. To illustrate this further, in Fig. 8 we plot the number of bacteria accumulated at the attractant source, B_S , which is the maximum of the bacterial profiles shown in Fig. S3, as a function of time for chemotactic and chemotactic-chemokinetic populations. The plot shows accumulation with ($\zeta > 0$ in (12e)) or without ($\zeta = 0$) account for the temporal perturbation to the chemotactic response. In the case of a purely chemotactic population, the predicted amount of bacteria accumulated at the source is lower for a model that ignores the temporal perturbation than for one that includes it. Chemokinesis, on the other hand, reduces the relative effect of temporal perturbation so much that there is very little difference between model predictions with $\zeta = 0$ and $\zeta > 0$.

These results suggest that a chemokinetic population

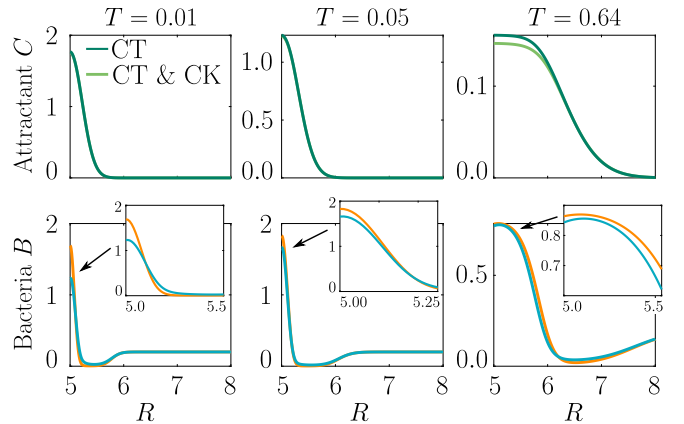


FIG. 7: Diffusing attractant from a transient source. Bacterial populations (bottom row) are attracted to source of diffusing attractant (top row). The chemokinetic-chemotactic population (orange curve) shows a faster and stronger accumulation than the purely chemotactic population (blue curve). Parameters $H = 3.5$, $K_S = 1$, $N = 0.5$, $K_\chi = 0.53$, $\delta_0 = 50$, $\eta = 2$, $\omega = 0.2$, $n = 1$, $T = 0.01, 0.05, 0.64$; no bacterial growth.

might be able to overtake purely chemotactic competitors in response to a sudden nutrient release. While the difference observed in Fig. 8 of at most $\sim 12\%$ may seem small, a corresponding boost to the growth rate can be sufficient to outcompete a purely chemotactic strain within a few generations. Chemokinesis could be particularly beneficial in nutrient-limited environments. When nutrient concentrations are low, increasing swimming speed provides no benefit to bacteria. However, in the event of a sudden nutrient burst, it can be efficient for bacteria to increase their swimming speed, maximising accumulation at high nutrient concentrations and thus nutrient uptake. In such transient nutrient landscapes, we have further shown that chemokinesis can furthermore reduce the adverse effect that a temporal change in attractant profile can have on the chemotactic response.

DISCUSSION

Chemokinesis is a known response for many environmentally relevant bacteria, yet its consequences for bacterial population dynamics have been little explored. In this work, using a modified Keller-Segel continuum model we have shown how chemokinesis significantly affects both the dynamics and steady-states of bacterial populations capable of chemotactic and chemokinetic behaviour. Our model incorporates the effects of a concentration dependent speed, including an increase in the chemotactic sensitivity, and a recently suggested modification to the chemotactic response in dynamic environments [15],

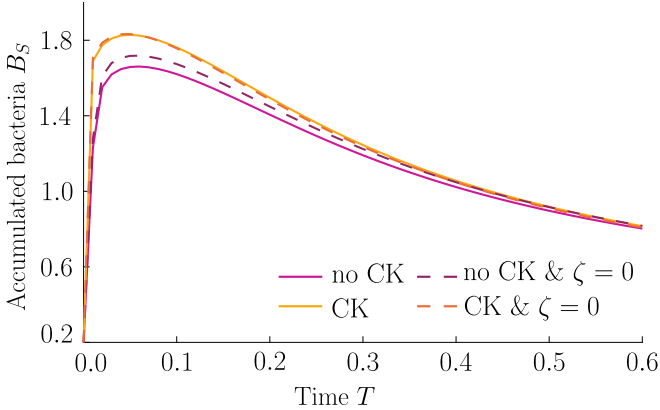


FIG. 8: Accumulation at a transient source. The bacterial accumulation at the source is reduced due to the reduced drift V_χ if the transient nature of the attractant profile is taken into account (i.e. $\zeta \neq 0$). Chemokinesis (CK) mitigates for this effect. Parameters $H = 3.5$, $K_S = 1$, $N = 0.5$, $K_\chi = 0.53$, $\delta_0 = 50$, $\zeta = 8.164 \cdot 10^{-3}$, $\eta = 2$ ($\eta = 0$ if no CK), $\omega = 0.2$, $n = 1$; no bacterial growth. If V_χ includes the effect of transient source, $\zeta = 8.164 \cdot 10^{-3}$, otherwise $\zeta = 0$.

which was derived adapting the microscopic model first suggested by de Gennes [17].

We have solved our model numerically to explore the effect of chemokinesis on migration and accumulation in experimentally realistic gradients. In a fixed attractant gradient, our results show that chemokinesis can lead to two subpopulations travelling at different speeds, with the slower one being held back by the chemokinetic drift. In the case of agar plate migration, where bacteria inoculated onto the plate generate their own gradient by consuming nutrients, we find that populations with chemokinesis migrate out from the inoculation point in waves that are faster, but broader than purely chemotactic migrating populations. It is possible that this broadening might explain why the classic chemotactic Adler bands observed for *E. coli* [20] are not observed for chemokinetic soil bacteria such as *Sinorhizobium meliloti* [21, 22]. Furthermore, chemokinesis increases the population growth significantly.

Our simulations also considered the case of a transient source of nutrients, e.g., a lysed alga. In this case, our results show how bacteria with chemokinesis and chemotaxis accumulate faster and more strongly around the source, while concentrations of nutrients are high, with respect to purely chemotactic bacteria. This chemokinetic advantage is both due to the enhanced migration discussed in the previous examples, but also to the fact that chemokinesis mitigates the perturbation to the chemotactic response due to the transient nature of the attractant profile. We note that, while our model includes the effect of transient chemical fields on tumbles,

it does not include a recently modelled effect of chemokinesis on the precision of chemosensing [25]. It will be interesting to include this additional effect, which could lead to further enhancements in chemokinetic accumulations, in future elaborations of our model.

The predictions of our model include several interesting qualitative effects, such as the slower subpopulation in the fixed attractant profile, which should be tested experimentally. For example, a recently developed *E. coli* system with a swimming speed that is independently controlled via light [19] could be used to engineer populations with chemotaxis, and chemotaxis and chemokinesis.

Future theoretical investigations would benefit significantly from the experimental measurement of the chemokinetic response function relating swimming speed and local attractant concentration. In this work we assumed a smooth change from a reference speed to an increased speed, where the degree of change in swimming speed changed with a single parameter. As we have shown, a very steep change in swimming speed (e.g. in form of a step change as assumed previously [8, 11]), could actually inhibit chemotaxis rather than promote it. Experimental work so far has been restricted to measurements at very few different attractant concentrations, which makes it difficult to deduce a functional relationship between speed and attractant concentration. Thus, further work is required to determine the function $v(c)$ for chemokinetic bacterial species. Such measurements would also allow elucidation of the rate of adaptation, i.e. how quickly the swimming speed adapts to its new value both for an increase and decrease in attractant concentration, and which we have here assumed instantaneous. However, a desensitisation, as observed for chemotaxis if the attractant concentration is continuously increased, seems to be absent for chemokinesis, at least in the case of *Rhodobacter sphaeroides* [26].

FUNDING

We acknowledge financial support from EPSRC EP/L504920/1 and EP/N509620/1 (T.J.) and the Winston Programme for the Physics of Sustainability (T.J., O.A.C.), and funding from the European Union's Horizon 2020 research and innovation programme under the Marie Skłodowska-Curie grant agreement No 798411 (F.J.P.).

Chemotactic drift and sensitivity

We follow the approach of [16, 17] to derive new relations for the chemotactic drift speed V_χ and sensitivity parameter χ for bacteria undergoing chemotaxis and chemokinesis in dynamic environments, connecting the

macroscopic parameter χ with the microscopic swimming speed v and tumbling rate α .

As the tumbling frequency follows an exponential distribution, tumbling events can be treated as independent events of a Poisson process with rate

$$\begin{aligned}\alpha(t) &= \alpha_0 \left(1 - \int_{-\infty}^t dt' K(t-t') f_\chi(x(t')) \right) \\ &\equiv \alpha_0(1 - \Delta(t)),\end{aligned}\quad (19)$$

where α_0 is the tumbling rate in the absence of a gradient and the concentration function was chosen in the main text as $f_\chi = c(x, t)/(c(x, t) + k_\chi)$. The response function $K(t)$ has only been measured for *E. coli* [27] and obeys $\int_0^\infty K(t) dt = 0$. The linear expression (19) assumes a shallow gradient, that is $\Delta(t) \ll 1$.

Considering a run that starts at $t = 0$, the probability density of a tumble event in the interval $[t, t+dt]$ is $\alpha(t) \exp(-\int_0^t dt' \alpha(t'))$. The mean run duration is given by

$$\tau = \left\langle \int_0^\infty \alpha(t) \exp \left(- \int_0^t dt' \alpha(t') \right) t dt \right\rangle, \quad (20)$$

where angled brackets denote averaging over all possible bacterial swimming paths, as the tumble rate is path dependent. Then, performing a change of variables in the memory integral (19) by defining $u = t - t'$, and recalling the assumption $\Delta(t) \ll 1$, yields

$$\begin{aligned}\tau &= \frac{1}{\alpha_0} + \alpha_0 \int_0^\infty dt e^{-\alpha_0 t} \times \\ &\quad \left\langle \int_0^t dt' \int_0^\infty du K(u) f_\chi(x(t'-u)) \right\rangle.\end{aligned}\quad (21)$$

Next, as the time interval of interest is small compared to the gradient variations, we can Taylor expand the concentration function above a reference position and time:

$$f_\chi(x(t-u)) \approx \text{const} + x(t-u) \nabla f_\chi |_{t=0} + (t-u) \partial_t f_\chi |_{x(t=0)}. \quad (22)$$

We note that the constant term does not influence the integral in (21), since the response function $K(u)$ integrates to zero. Further analysis is simplified by considering the special response function $K(u) = A\delta(u-\theta)$, where θ is a single delay time [17]. Equation (21) then becomes

$$\begin{aligned}\tau &\approx \frac{1}{\alpha_0} + A\alpha_0 \int_0^\infty dt e^{-\alpha_0 t} \times \\ &\quad \left\langle \int_0^t \{x(t'-\theta) \nabla f_\chi + (t'-\theta) \partial_t f_\chi |_{x(t')} \} dt' \right\rangle.\end{aligned}\quad (23)$$

Then, following [17], we notice that the position of a bacterium is, when averaging over paths, not correlated to the velocity for times $t-\theta < 0$, which precede a run. On the other hand, we can write $x(t-\theta) = \pm v(x)(t-\theta)$ for

$t-\theta > 0$, where $\pm v(x)$ is the speed up/down a gradient (assumed constant during a run). Similarly, the contribution from the temporal gradient $\partial_t f_\chi |_{x(t)}$ averages to zero for times prior to a run, while during a run it is positive for paths directed up the spatial gradient, and negative for paths down this gradient. This reflects the effective gradient perceived by the bacterium for temporally varying concentration profiles [15]. We can thus write the mean run durations up (R) and down (L) the gradient as

$$\begin{aligned}\tau^{L,R} &\approx \frac{1}{\alpha_0} + A\alpha_0 \int_0^\infty dt e^{-\alpha_0 t} \times \\ &\quad \int_0^t \{ \pm v(x) |\nabla f_\chi| \mp |\partial_t f_\chi| \} (t' - \theta) dt',\end{aligned}\quad (24)$$

which, taking $|\partial_t f_\chi|$ out of the integrals since f_χ varies on times much slower than the active interval, can be integrated twice to obtain

$$\tau^{L,R} \approx \frac{1}{\alpha_0} \pm \frac{v(x)}{\alpha_0^2} \left[|\nabla f_\chi| - \frac{1}{v(x)} |\partial_t f_\chi| \right] A e^{-\alpha_0 \theta}. \quad (25)$$

Extending to general response function $K(\theta)$ with a distribution of delays [17], equation (25) becomes

$$\tau^{L,R} \approx \frac{1}{\alpha_0} \pm \frac{v(x)}{\alpha_0^2} \left[|\nabla f_\chi| - \frac{1}{v(x)} |\partial_t f_\chi| \right] \int_0^\infty d\theta K(\theta) e^{\alpha_0 \theta}. \quad (26)$$

Since $\alpha_{L,R} = 1/\tau_{L,R}$ and (see main text)

$$V_\chi = v(x) \frac{\alpha_L - \alpha_R}{\alpha_R - \alpha_L}, \quad (27)$$

we then arrive at an expression for the chemotactic drift

$$V_\chi = \frac{v(x)^2}{\alpha_0} \beta \left[|\nabla f_\chi| - \frac{1}{v(x)} |\partial_t f_\chi| \right], \quad (28)$$

where we have defined the constant $\beta = \int_0^\infty d\theta K(\theta) e^{-\alpha_0 \theta}$. The standard definition of the chemotactic sensitivity is obtained from the empirical drift $V_\chi = \chi |\nabla f_\chi|$, where as previously χ is the chemotactic sensitivity. We extend here the definition to include temporal gradients, and define

$$\chi(x) = \frac{v(x)^2}{\alpha_0} \beta, \quad (29)$$

so that chemotactic drift is given by Eq. (4) in the main text. In the absence of chemokinetic alterations to the swimming speed, the sensitivity is simply

$$\chi_0 = \frac{v_0^2}{\alpha_0} \beta, \quad (30)$$

where subscripts denote a constant swimming speed. Dividing (29) by (30) provides relationship (7) in the main text.

Numerical solution

A finite difference scheme was chosen to compute the numerical solution of the system of PDEs (12). The domain Ω is represented by a vector of M equally spaced grid points, X_1, \dots, X_M . A fourth order scheme in space and a first order scheme in time are used to approximate the derivatives. Homogeneous Neumann boundary conditions are imposed for both substrate and bacterial concentration, i.e. $\frac{\partial C}{\partial X}|_{X=1,M} = 0$ and $\frac{\partial B}{\partial X}|_{X=1,M} = 0$.

In the case of steady attractant gradient (Fig. 3 and Fig. 4) the initial attractant distribution is $C(X, 0) = 0.01X$, while the bacteria are uniformly distributed $B(X, 0) = 1.0$. For the self-generated gradient (Fig. S2 and Fig. 6) we assume a Gaussian bacterial inoculum, $B(R, 0) = \exp(-R^2/\sigma^2)$, with a corresponding attractant distribution, $C(R, 0) = 1 - \exp(-R^2/\sigma^2)$ [16]. Finally, for Fig. S3 and Fig. 8 the bacteria are initially uniformly distributed $B(R, 0) = 0.2$, while the attractant distribution is $C(R, 0) = 1/\sqrt{0.16\pi N} \exp(-R^2/0.16N)$. The parameters used in the non-dimensional model are summarised in Table I. The parameters are mostly based on literature values for *E. coli*. The values for the chemokinetic response (η , ω , n) are chosen to illustrate the response. The parameters used to produce the figures in the main text were chosen to illustrate the effect of chemokinesis best. As a comparison, other parameter combinations are given in the Supplementary Material.

SUPPLEMENTARY MATERIALS

Additional simulations

We present further simulation results for the scenarios described in the manuscript by varying crucial and unknown parameters determining the bacterial response. As the chemokinetic response function is unknown, these include the strength of the chemokinetic speed increase η , the half-saturation concentration of the chemokinetic response ω and the Hill factor n as well as the strength of the chemotactic response δ_0 .

Steady linear gradient

The effect of modifying the chemotactic sensitivity δ_0 and the chemokinetic parameters η and ω is shown in Figure S1.

Self-generated gradient

The effect of varying the Hill parameter n of the chemokinetic function $V(C) = 1 + \frac{\eta C^n}{C^n + \omega^n}$ is shown

TABLE I: Parameters used in simulations. Please see main text for parameter definitions.

Parameter	Value	Figure	Reference
H	0.0	3, 4	-
	3.5	S2, S3, 8	[16]
N	0.0	3, 4	-
	0.5	S2, S3, 8	[16]
δ_0	50.0	3, 4, S3	-
	105.0	S2	[16]
ω	0.2	3, 4, S3	-
	0.5	S2	-
η	2.0	3, 4, S3	-
	0.5	S2	[5]
n	1	4, S3	-
	5	3, 4, S2	-
	10	4	-
	40	4	-
ζ	0.0	3, 4, S2	-
	$8.164 \cdot 10^{-3}$	S3	[16]
K_S	1.0	3, 4, S2, S3	[16]
K_χ	0.53	3, 4, S2, S3	[16]
S	1.0	S3 8	

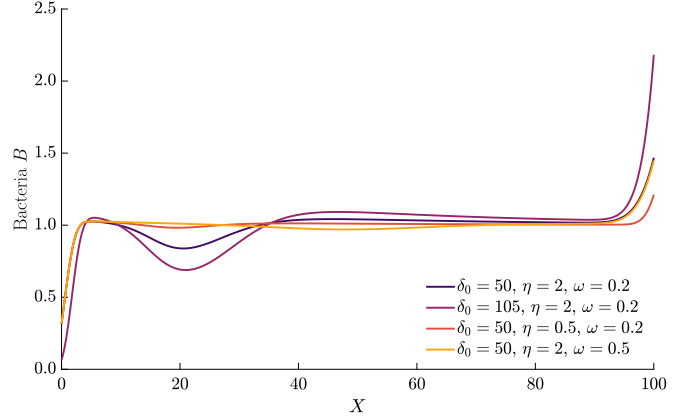


FIG. S1: Bacterial response to a fixed linear attractant gradient as in Fig 3 in the main paper but with varying parameters ($T = 1$).

in Figure S2(a). Figure S2(b) illustrates the effect of the chemotactic sensitivity δ_0 and the chemokinetic parameters ω and η .

Transient source

The parameters used in the main text are the same as those used for the steady linear attractant gradient. The results of a simulation that uses the parameters of the

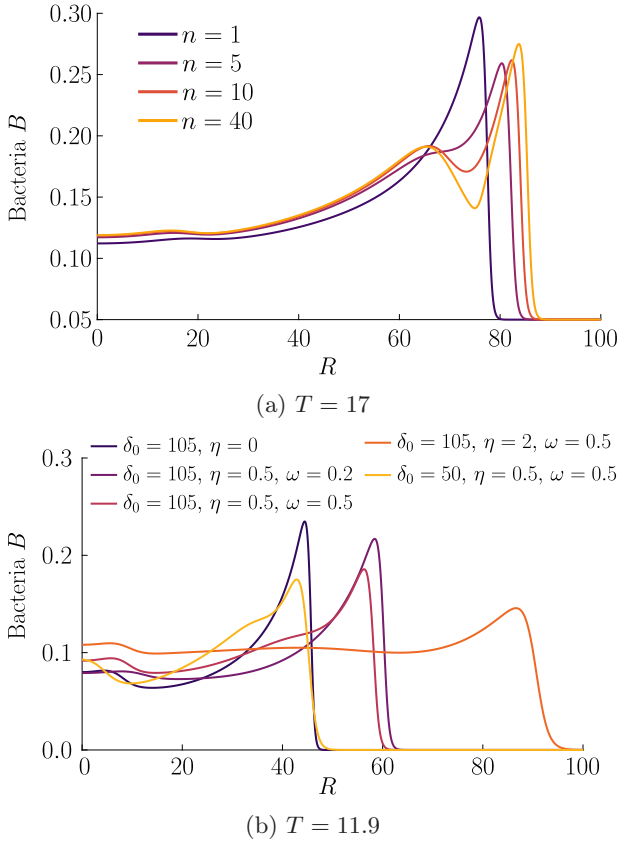


FIG. S2: Bacterial response to a self-generated attractant gradient as in Fig. 5 in the main text but with varying parameters. (a) Varying the Hill parameter in the chemokinetic response function changes the bacterial density at $T = 17$ (corresponds to the last column in Fig. 5 in the main text). (b) Varying chemotactic and chemokinetic parameters δ_0 , η and ω at $T = 11.9$, where a simulation using the parameters from the main paper is included as a comparison for this time step.

self-generated attractant gradient instead are shown in Figure S3.

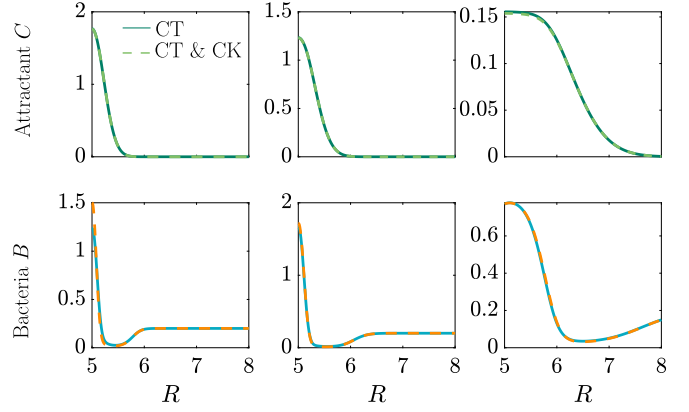


FIG. S3: Diffusing attractant from a transient source. Bacterial populations (bottom row) are attracted to source of diffusing attractant (top row). The chemokinetic-chemotactic population (orange curve) shows a faster and stronger accumulation than the purely chemotactic population (blue curve). Parameters $H = 3.5$, $K_S = 1$, $N = 0.5$, $K_\chi = 0.53$, $\delta_0 = 50$, $\eta = 0.5$, $\omega = 0.5$, $n = 1$, $T = 0.01, 0.05, 0.64$; no bacterial growth.

- [5] Garren M, Son K, Raina JB, Rusconi R, Menolascina F, Shapiro OH, et al. A bacterial pathogen uses dimethylsulfoniopropionate as a cue to target heat-stressed corals. ISME J. 2014;8(5):999–1007.
- [6] Armitage JP, Schmitt R. Bacterial chemotaxis: *Rhodobacter sphaeroides* and *Sinorhizobium meliloti* – variations on a theme? Microbiology. 1997;143:3671–3682.
- [7] Barbara GM, Mitchell JG. Bacterial tracking of motile algae. FEMS Microbiology Ecology. 2003;44(1):79–87.
- [8] Garren M, Son K, Tout J, Seymour JR, Stocker R. Temperature-induced behavioral switches in a bacterial coral pathogen. ISME J. 2016;10:1363–1372.
- [9] Walther A, Müller AH. Janus particles: synthesis, self-assembly, physical properties, and applications. Chem Rev. 2013;113(7):5194–5261.
- [10] Howse JR, Jones RA, Ryan AJ, Gough T, Vafabakhsh R, Golestanian R. Self-motile colloidal particles: from directed propulsion to random walk. Phys Rev Lett. 2007;99(4):048102.
- [11] Son K, Menolascina F, Stocker R. Speed-dependent chemotactic precision in marine bacteria. Proc Natl Acad Sci USA. 2016;113(31):1–6.
- [12] Jackson GA. Simulating chemosensory responses of marine microorganisms. Limnol Oceanogr. 1987;32(6):1253–1266.
- [13] Schnitzer MJ. Theory of continuum random walks and application to chemotaxis. Phys Rev E. 1993;48(4):2553–2568.
- [14] Cates ME. Diffusive transport without detailed balance in motile bacteria: does microbiology need statistical physics? Rep Prog Phys. 2012;75(4):042601.
- [15] Hein AM, Brumley DR, Carrara F, Stocker R, Levin SA. Physical limits on bacterial navigation in dynamic environments. J Royal Soc Interface. 2016;13(114):20150844.

* tj295@cam.ac.uk

† oac24@cam.ac.uk

- [1] Berg HC. Random walks in biology. Princeton University Press; 1993.
- [2] Berg HC. *E. coli* in motion. Springer; 2004.
- [3] Tindall MJ, Maini PK, Porter SL, Armitage JP. Overview of Mathematical Approaches Used to Model Bacterial Chemotaxis II: Bacterial Populations. B Math Biol. 2008;70:1570–1607.
- [4] Barbara GM, Mitchell JG. Marine bacterial organisation around point-like sources of amino acids. FEMS Microbiology Ecology. 2003;43(1):99–109.

- [16] Croze OA, Ferguson GP, Cates ME, Poon WCK. Migration of chemotactic bacteria in soft agar: Role of gel concentration. *Biophys J.* 2011;101(3):525–534.
- [17] De Gennes PG. Chemotaxis: The role of internal delays. *Eur Biophys J.* 2004;33(8):691–693.
- [18] Rusconi R, Garren M, Stocker R. Microfluidics Expanding the Frontiers of Microbial Ecology. *Annu Rev Biophys.* 2014;43(1):65–91.
- [19] Arlt J, Martinez VA, Dawson A, Pilizota T, Poon WC. Painting with light-powered bacteria. *Nat Commun.* 2018;9(1):768.
- [20] Adler J. Chemotaxis in bacteria. *Science.* 1966;153:708–716.
- [21] Platzer J, Sterr W, Hausmann M, Schmitt R. Three genes of a motility operon and their role in flagellar rotary speed variation in *Rhizobium meliloti*. *J Bacteriol.* 1997;179(20):6391–6399.
- [22] Meier VM, Muschler P, Scharf BE. Functional analysis of nine putative chemoreceptor proteins in *Sinorhizobium meliloti*. *J Bacteriol.* 2007;189(5):1816–1826.
- [23] Smriga S, Fernandez VI, Mitchell JG, Stocker R. Chemotaxis toward phytoplankton drives organic matter partitioning among marine bacteria. *Proc Natl Acad Sci USA.* 2016;113(6):1576–1581.
- [24] Stocker R, Seymour JR, Samadani A, Hunt DE, Polz MF. Rapid chemotactic response enables marine bacteria to exploit ephemeral microscale nutrient patches. *Proc Natl Acad Sci USA.* 2008;105(11):4209–4214.
- [25] Brumley DR, Carrara F, Hein AM, Yawata Y, Levin SA, Stocker R. Bacteria push the limits of chemotactic precision to navigate dynamic chemical gradients. *Proc Natl Acad Sci USA.* 2019;116(22):10792–10797.
- [26] Packer HL, Armitage JP. The chemokinetic and chemotactic behavior of *Rhodobacter sphaeroides*: Two independent responses. *J Bacteriol.* 1994;176(1):206–212.
- [27] Segall JE, Block SM, Berg HC. Temporal comparisons in bacterial chemotaxis. *Proc Natl Acad Sci USA.* 1986;83(23):8987–8991.